

Relation between heterogeneous frozen regions in supercooled liquids and non-Debye spectrum in the corresponding glasses

Matteo Paoluzzi^{1,*}, Luca Angelani^{1,2}, Giorgio Parisi^{1,3,4}, and Giancarlo Ruocco^{1,5}

¹ Dipartimento di Fisica, Sapienza Università di Roma, Piazzale A. Moro 2, I-00185, Rome, Italy

² ISC-CNR, Institute for Complex Systems, Piazzale A. Moro 2, I-00185 Rome, Italy

³ Nanotec-CNR, UOS Rome, Sapienza Università di Roma, Piazzale A. Moro 2, I-00185, Rome, Italy

⁴ INFN-Sezione di Roma 1, Piazzale A. Moro 2, I-00185, Rome

⁵ Center for Life Nano Science, Istituto Italiano di Tecnologia, Viale Regina Elena 291, I-00161, Rome, Italy

Recent molecular dynamics simulation of glasses brought compelling evidenced of the existence – besides the phonons that are Goldstone (G) vibrational modes– of non-Goldstone (nG) modes. Different strategies have been exploited to modify the relative weight of G to nG modes in the vibrational density of states $D(\omega)$, as for example by freezing the dynamics of a fraction p of particles. Here we first show that the nG to G ratio —as measured by the behavior of $D(\omega)$ at low frequency: $D(\omega) \sim \omega^{s(T^*)}$ with $2 \leq s(T^*) \leq 4$ — is enhanced when vibrations are associated with an inherent structure deep in the energy landscape, obtained by a fast quench of a supercooled liquid equilibrated at T^* . Secondly, by comparing $s(T^*)$ with the same quantity obtained by pinning p particles, $s(p)$, we suggest that $s(T^*)$ reflects the presence of dynamical heterogeneous regions of size $\xi^3 \sim p$. Finally, we provide an estimate of ξ a function of T^* , finding a mild power law divergence, $\xi \sim (T^* - T_d)^{-\alpha/3}$, at the dynamical crossover temperature T_d , with α in the range [0.8, 1.0].

Introduction. At small enough frequencies ω , the density of states $D(\omega)$ of three dimensional disordered media like structural glasses follows Debye's law $D(\omega) \sim \omega^2$. This is because at large enough length scale glasses are continuum media and thus phonons dominate the low frequency spectrum [1]. However, compared with crystals, glasses show thermodynamic anomalies at low temperatures. For instance, the thermal conductivity $\kappa(T)$ scales with T^2 [2] instead T^3 , as predicted by Debye's law [1]. Moreover, also the specific heat C_v below 1 K deviates from Debye's law acquiring a linear dependency on T [2]. Remarkably, these anomalies are shared by a broad class of glassy systems providing evidences of universality.

As it has been noticed in Ref. [3], in disordered media and small ω , $D(\omega)$ takes contributions from both, extended Goldstone bosons, e. g., phonons in structural glasses or spin-waves in Heisenberg spin glasses, and non-Goldstone modes, i. e., excitations that are not generated by the spontaneous symmetry breaking of a continuous symmetry. The Goldstone contribution gives rise to the Debye spectrum $D(\omega) \sim \omega^{d-1}$, with d the number of spatial dimensions. The non-Goldstone sector is still soft, i.e., normal modes whose density of states vanishes as a power law $D(\omega) \sim \omega^s$ [3], but it is populated by localized modes. Only in the last few years, thanks to the possibility of eliminating Goldstone bosons from the low-energy spectrum [4, 5] or discriminating non-extended modes from the extended ones [6], it has been possible to observe numerically the non-Goldstone sector in models of structural glasses [6–8] and in Heisenberg spin-glass [4] obtaining that, in agreement with the arguments suggested in Ref. [3], the density of states of the non-Goldstone contribution scales with the exponent $s = 4$.

In a previous work, analyzing a not-so-large sample ($N \leq 10^4$) we showed that a population of soft-localized modes with density of states $\sim \omega^{s(p)}$ and $2 \leq s(p) \leq 4$ emerges in the low-frequency spectrum of a three dimensional model of glass when a fraction p of particles are randomly frozen [9]. In particular, the value of the effective exponent $s(p)$ starts from $s=2$ at $p=0$ and approaches 4 above a threshold p_{th} value that is of the order of 50% of frozen particles. This result can be rationalized by noticing that pinning even a small number of particles shifts the extended modes (phonons) towards high frequencies, leaving untouched the localized modes, which live in between the pinned particles.

In this paper we study the properties of $D(\omega)$ of a model glass lying in the inherent configuration, i. e., minima of the potential energy populated at $T=0$. The latter, employed for computing the dynamical matrix, has been obtained by a fast quench starting from a configuration that is at equilibrium at finite, parental, temperature T^* .

As a first result, we observe a progressive attenuation of the Debye spectrum in favor of the non-Debye one as T^* approaches from above the dynamical crossover temperature T_d . In particular, $s=2$ at $T^* \gg T_d$, it increases by decreasing T^* and it saturates to $s = 4$ right above T_d . This crossover between Debye to non-Debye is accompanied by a progressively localization of the normal modes below the Boson peak. The behaviour of $s(T^*)$ mirrors that of $s(p)$ observed in [9], indicating an increase in size of the frozen heterogeneous region on lowering T^* and suggesting a way to measure the size of these regions.

For making quantitatively in contact the suppression of extended excitations with the rising of spatially heterogeneous localization regions, we perform a mapping between the properties of the inherent states of the randomly pinned system at high parental temperatures, i. e., ($T^* = \infty, p$), with the inherent structures of the same

*Electronic address: Matteo.Paoluzzi@roma1.infn.it

system at low temperatures without frozen particles. i. e., $(T^*, p = 0)$, and same system size N . In particular, looking at the solution of $s(T^*, p = 0) = s(T^* = \infty, p)$ we show that the resulting curve $p(T^*)$ provides an estimate for the correlation length ξ , being $\xi = (pN/\rho)^{1/3}$. We are then able to extract the behavior of ξ as a function of parental temperature i.e. of the equilibrium temperature of the supercooled liquid. It turns out that ξ is compatible with a power law divergence at T_d , $\xi^3 = (T^* - T_d)^{-\alpha}$ and α not far from one.

The previous result has been confirmed analysing a second quantity beside $s(T^*, p)$. Specifically we measured the distance Δr travelled by each particles between the instantaneous equilibrated configuration at $T = T^*$ and the inherent configuration at $T = 0$ during the quenching process. The distribution of Δr depends on both T^* and p , and their variances $\sigma(T^*, p)$ have been used to derive $p(T^*)$ in a second, independent, way via $\sigma(T^*, p = 0) = \sigma(T^* = \infty, p)$.

Model and Observables. We consider a three dimensional system composed of a 50 : 50 binary mixture of N soft sphere confined in a cubic box of side L with periodic boundary conditions and interacting through a pure repulsive pairwise potential [10, 11]. We label large particles with A and the small ones with B . The total number of particle reads $N = N_A + N_B$ and the corresponding density is $\rho = N/L^3$. The radii are σ_A and σ_B with $\sigma_A/\sigma_B = 1.2$ and $\sigma_A + \sigma_B \equiv \sigma = 1$ [11]. The side of the box is $L = N^{1/3}$ such that $\rho = 1$. Indicating with \mathbf{r}_i the position of the particle i , with $i = 1, \dots, N$, two particles i, j interact via the potential $\phi(r_{ij}) = \epsilon((\sigma_i + \sigma_j)/r_{ij})^{12} + k_0 + k_2 r_{ij}^2$, where $r_{ij} \equiv |\mathbf{r}_i - \mathbf{r}_j|$. We impose a cutoff to the potential at $r_c = \sqrt{3}\sigma$ in a way that $\phi(r) = 0$ for $r > r_c$. The coefficient k_0 and k_2 guaranty continuity to $\phi(r)$ up to the first derivative at $r = r_c$. For the dynamics, we have considered hybrid Brownian/Swap Monte Carlo simulations obtained combining the numerical integration of the equations of motion with Swap Montecarlo moves [11]. In particular, in order to generate thermalized configurations, we propose an update of the system according to swap moves every 2×10^3 time steps. We consider system sizes $N = 10^3, 12^3$ and averaging over 400 configurations. In the following we report all quantities in reduced units considering $\sigma = \epsilon = \mu = 1$, where μ is the mobility of the Brownian particles. The Mode-Coupling Temperature of the model T_d has been evaluated considering a power law fit for the relaxation time τ_α of the self correlation function, $\tau_\alpha \sim (T - T_d)^{-b}$. For computing T_d , we consider the dynamical evolution of the system without swap moves.

After thermalization, we compute the corresponding inherent structures through the Limited-memory Broyden-Fletcher-Goldfarb-Shanno algorithm [12]. Let \mathbf{r} be a configuration of the system, i. e., $\mathbf{r} \equiv (\mathbf{r}_1, \dots, \mathbf{r}_N)$. The mechanical energy of the configuration \mathbf{r} is $E[\mathbf{r}] = \sum_{i < j} \phi(r_{ij})$. We indicate with $\mathbf{r}^0 \equiv (\mathbf{r}_1^0, \dots, \mathbf{r}_N^0)$ the configuration that minimizes $E[\mathbf{r}]$, the spectrum of the harmonic oscillations around \mathbf{r}^0 is then obtained consider-

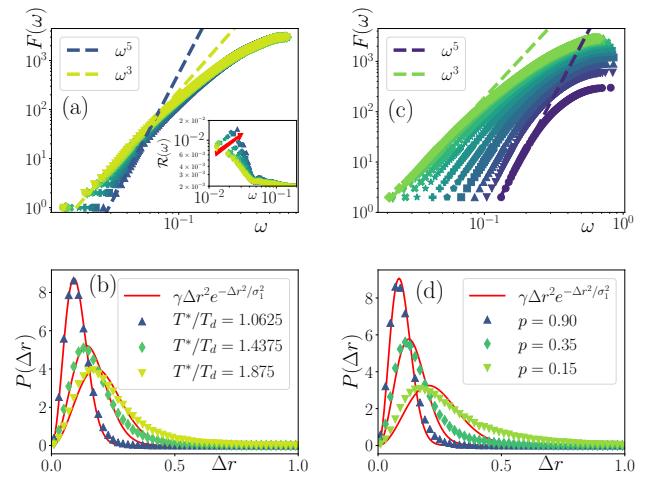


FIG. 1: (a) Cumulative density of states $F(\omega)$ as function of the parental temperature T^* for $N = 10^3$. Temperatures decrease from yellow to blue, $T^*/T_d = 1.875, 1.5625, 1.5, 1.4375, 1.375, 1.3125, 1.25, 1.1875, 1.125, 1.06$. Inset: Inverse participation ratio $\mathcal{R}(\omega)$. (b) Probability distribution function $P(\Delta r)$ of the total displacement Δr by varying temperature. (c) Cumulative function $F(\omega)$ as the fraction of frozen particles p increases at high temperature $T/T_d = 3.125$. p increases from green to violet, $p = 0.05, 0.1, 0.2, 0.3, 0.4, 0.5, 0.6, 0.7, 0.8, 0.9$. (d) $P(\Delta r)$ at $T/T_d = 3.125$ as p increases from green to blue.

ing a perturbed configuration $\mathbf{r} = \mathbf{r}^0 + \delta\mathbf{r}$. The mechanical energy now reads $E[\delta\mathbf{r}] = E[\mathbf{r}^0] + \Delta E$ with $\Delta E \equiv \frac{1}{2} \sum_{i,j} \sum_{\mu,\nu} \delta r_i^\mu M_{ij}^{\mu\nu} \delta r_j^\nu$ with $M_{ij}^{\mu\nu}$ the elements Hessian matrix \mathbf{M} , where latin indices $i, j = 1, \dots, N$ indicate the particles and greek symbols $\nu, \mu = 1, \dots, 3$ the cartesian coordinates. For estimating the correlation length ξ , we also considered configurations where a finite number of particles pN , with $p \in [0, 1]$ the particle fraction, are maintained frozen during the minimization of $E[\mathbf{r}]$. The details about the minimization of $E[\mathbf{r}]$ with pinned particles can be found in Ref. [9]. We have computed all the $3N$ eigenvalues λ_κ , with $\kappa = 1, \dots, 3N$, using *gsl-GNU libraries* for sizes up to $N = 12^3$. The corresponding eigenvalues of \mathbf{M} are $\omega_\kappa^2 = \lambda_\kappa$.

We focus our attention on the cumulative $F(\omega) = \int_0^\omega d\omega' D(\omega')$, where $D(\omega) = \mathcal{N}^{-1} \sum_\kappa \delta(\omega - \omega_\kappa)$ is the density of states. \mathcal{N} is the number of non-zero modes that is $3N - 3$ for translational invariant systems. We also computed the distribution $P(\Delta r)$, with $P(\Delta r) = N^{-1} \sum_i \delta(\Delta r - \Delta r_i)$, and $\Delta r_i \equiv |\mathbf{r}_i - \mathbf{r}_i^0|$ the total displacement covered by the particle i for reaching the inherent configuration starting from the equilibrated one.

The localization properties of the normal-modes have been investigated through the inverse participation ratio $\mathcal{R}(\omega)$ defined as $\mathcal{R}(\omega) \equiv \sum_i |\mathbf{e}_i(\omega)|^4 / (\sum_i |\mathbf{e}_i(\omega)|^2)^2$ where $\mathbf{e}_i(\omega)$ is the eigenvector of the mode ω [13]. For a mode ω completely localised on a single particle, one has $\mathcal{R}(\omega) = 1$, while a mode extended over all the particles

corresponds to $\mathcal{R}(\omega) \sim N^{-1}$.

Results. Let us start with discussing the effect of the parental temperature on the cumulative function. $F(\omega)$ is shown in Fig. (1a) for different parental temperatures and system size $N = 10^3$. As one can see, approaching the dynamical temperature, i.e. $T^*/T_d \rightarrow 1$, the exponent of the low-frequency power law $F(\omega) \sim \omega^{s(T^*)+1}$ increases as temperature decreases departing from the Debye value $s = 2$ to higher values. As shown in Fig. (2a), $s+1 \rightarrow 5$ as $T^* \rightarrow T_d$. The exponents have been computed fitting the tail of $F(\omega)$ below the Boson peak [14, 15] with a power law. Since the Boson peak is populated by extended modes, we select the low-frequency sector through the \mathcal{R} value of the mode ω . As one can see in the inset of Fig. (1a), below $\omega \sim 0.04$, \mathcal{R} grows as frequency decreases. Moreover, in that region, \mathcal{R} grows with decreasing T (the red arrow goes in the direction of decreasing temperatures), indicating that low-frequency modes become more localized as temperature decreases. The situation is different above $\omega \sim 0.04$ where \mathcal{R} approaches the $1/N$ limit. It is worth noting that the latter modes populate the Boson peak and they remain extended no matter how far the system is from T_d . The increasing in $\mathcal{R}(\omega)$ and the behavior $F(\omega) \sim \omega^{1+s(T^*)}$ on lowering frequency is consistent with the presence of soft-localized modes.

In order to gain insight into the nature of the rearrangements made by the system for reaching the inherent configuration \mathbf{r}^0 , we have then computed the distribution $P(\Delta r)$ that is shown in Fig. (1b). As one can see, the distribution becomes peaked at lower and lower Δr values as temperature decreases indicating that particles in configurations at lower temperature turn to be more caged during minimisation. The red curves in Fig. (1b) are fits to $\gamma \Delta r^2 e^{-\Delta r^2/\sigma_1^2}$, with γ and σ_1 adjustable parameters. One can notice the presence of non-Gaussian tails at high temperatures that progressively disappear for $T^* \rightarrow T_d$. To be more quantitative, we have also computed the true variance σ_2 of the distribution $P(\Delta r)$, $\sigma_2(T^*)$ (see Fig. (2b,2d)).

A similar phenomenology is observed looking at the system at high T^* but including a fraction of frozen particle during the research of the inherent structure [9]. In particular, when the concentration of frozen particles is large enough, moving particles are caged by the non-moving ones. In this situation the Rayleigh-type density of states $D(\omega) \sim \omega^4$ dominates the low-energy spectrum [9]. In Fig. (1c) the cumulative $F(\omega)$ is shown at $T^*/T_d = 3.125$ by varying the fraction of frozen particles p , that increases from left to right. We have thus computed the distributions $P(\Delta r)$ when a fraction p of particles is maintained frozen, the results are shown in Fig. (1d). Again, the red curves are the gaussian fit. As one can appreciate, the behavior of $P(\Delta r)$ with increasing the fraction of frozen particles p is qualitatively the same obtained with decreasing temperature in the unpinned system. This is a strong indication that the same crossover from a spectrum dominated by soft-extended

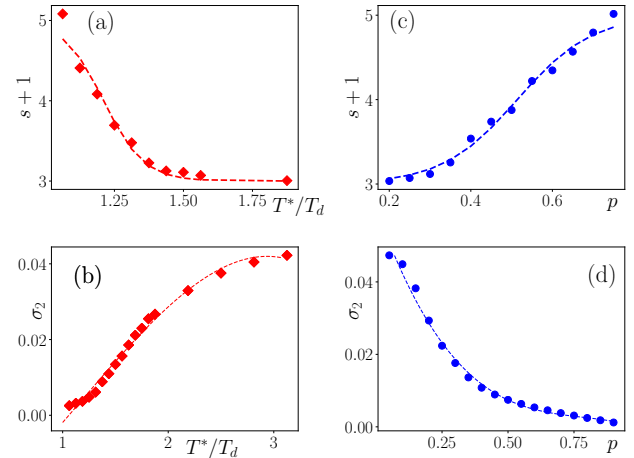


FIG. 2: (a) Slope s of the power law $F(\omega) \sim \omega^{s+1}$ as a function of the parental temperature T^* for $N = 10^3$. (b) Variance of the distribution $P(\Delta r)$ as a function of T^* . (c) Slope s as a function of p at $T^* = 3.125$ (d) Variance of the distribution $P(\Delta r)$ as a function of p at $T^* = 3.125$. Dashed lines are guides to the eye.

modes to soft-localized modes takes place in both protocols, i.e, decreasing parental temperature or increasing the fraction of pinned particles. The advantage of introducing randomly frozen particles lies in the fact that controlling p we are also controlling the typical size ξ of frozen regions. In order to define ξ , we notice that the number of frozen particles $N_p = pN$ is naturally proportional to the volume of frozen particles V_p , thus $\xi^3 \propto pN$.

In order to make quantitative progresses, we look at the curves $s(T^*)$ and $s(p)$ obtained from $F(\omega)$, as well as at $\sigma_1(T^*)$ and $\sigma_1(p)$ (or, equivalently, at $\sigma_2(T^*)$ and $\sigma_2(p)$) obtained from $P(\Delta r)$. As already noticed $s(T^*)$ increases with decreasing T^* : this behavior is reported in Fig. (2a). Similarly, the behaviour of $\sigma_2(T^*)$ as a function of T^* is reported in Fig. (2b). In panels (c) and (d) of the same figure we show the same observables as a function of the fraction of frozen particles p for configurations thermalised well above the dynamical temperature, i. e., $T^*/T_d = 3.125$.

We can thus provide a quantitative estimate of the behaviour of ξ as a function of T^* mapping the properties of the pinned system into the properties of the thermal system. In particular, we assume that, in a system where a fraction p of particles are frozen randomly in space, one introduces a correlation length $\xi \equiv \left(\frac{pN}{\rho}\right)^{1/3}$. For inferring the correlation length ξ in the real system, i. e., without artificially frozen particles, we invert the relation $\mathcal{O}(T^*, p = 0) = \mathcal{O}(T^* \gg T_d, p)$, where \mathcal{O} is a generic observable, obtaining a function $p(T^*) \equiv \xi^3(T^*)$. The results of our analysis are shown in Fig. (3) for system sizes $N = 10^3, 12^3$. Diamonds are obtained considering as observable \mathcal{O} the exponents of the power laws $s(T^*)$

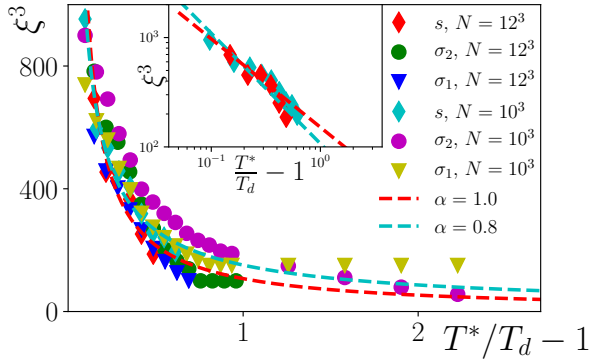


FIG. 3: Correlation length ξ^3 defined in the main text as a function of temperature T^* and estimated through different observables for $N = 10^3, 12^3$. Diamonds refer to $s(T^*, p = 0) = s(T^* = \infty, p)$ method, circles to $\sigma_2(T^*, p = 0) = \sigma_2(\infty, p)$, and triangles using σ_1 , i. e., fitting $P(\Delta r)$ to $\gamma \Delta r^2 e^{-\Delta r^2/\sigma_1^2}$ and thus considering $\sigma_1(T^*, p = 0) = \sigma_1(T^* = \infty, p)$. The inset highlights the behavior of ξ^3 computed through the exponent s for $N = 10^2, 10^3$, cyan and red symbols, respectively. Dashed lines are fits to the power law $(T^* - T_d)^{-\alpha}$ with $\alpha = 0.8$ (red) and $\alpha = 1.0$ (cyan).

and $s(p)$, i.e. $\mathcal{O} \equiv s$, circles refer to the true variance of the distribution $P(\Delta r)$, $\mathcal{O} \equiv \sigma_2$, and triangles are obtained considering the parameter σ_1 from the fit of $P(\Delta r)$ to a gaussian distribution ($\mathcal{O} \equiv \sigma_1$). The dashed curves are the power law $\xi^3 \sim (T^* - T_d)^{-\alpha}$. The exponent α has been computed considering $\mathcal{O} = s$ and data set $N = 10^3$ (cyan symbols), $N = 12^3$ (red symbols). We then obtain $\alpha_{max} = 1.0$ and $\alpha_{min} = 0.8$ for $N = 12^3, 10^3$, respectively, indicating that the exponent α varies in the range $\alpha \in [0.8, 1.0]$. As one can appreciate, different observables \mathcal{O} give estimate for ξ as a function of T^* that are in good agreement with each other.

Summary and Discussion. In this paper, we have explored the properties of the low-frequency excitations in a three-dimensional model glass obtained by fast quench from a well equilibrated super-cooled liquid configuration at $T = T^*$. The values of T^* spanned from high temperature down to the dynamical transition temperature T_d . We have shown that quasi-localized soft modes progressively populate the low-frequency spectrum. The density of states of these *glassy modes* follows a scaling law $\omega^{s(T^*)}$ with $2 \leq s(T^*) \leq 4$. In particular, far away from the dynamical transition, the low-frequency spectrum below the Boson peak is well described by Debye's law, i. e., $s(T^*) = 2$. As T^* decreases, $D(\omega)$ at small ω is still power law with an exponent that is temperature dependent and deviates from Debye's law. In particular, s starts to increase its value and $s(T^*) \rightarrow 4$ for $T^* \rightarrow T_d$. As shown here and also before in Ref. [9], the same quasi-logistic growth in s is observed when, instead of varying

the parental temperature, we introduce a fraction p of frozen particles. In particular, the spectrum of the low-energy excitations below the Boson peak remain gapless and progressively deviates from Debye's law following a scaling $\omega^{s(p)}$, and $2 \leq s(p) \leq 4$. In this case, $s(p)$ increases as p increases and $s \rightarrow 4$ above a threshold value $p_{th} \sim 0.5$. Pinned particles have been often adopted for gaining insight into glassy dynamics in both, analytical models [16–19] and numerical simulations [20–27]. Here, in parallel with the study as a function of the parental temperature, we used random pinning to gain insight into the T dependence of the correlation length ξ .

The emerging phenomenology is consistent with a picture of heterogeneous regions where particles experienced different mobilities [28–30]. An estimate of the typical linear size ξ of these heterogeneous regions is provided in the pinned system by $p^{1/3}$, in three spatial dimensions. Since the correlation length ξ can be tuned through the fraction of frozen particles p , random pinning provide a powerful tool not only for gaining insight into the low-frequency spectrum, i. e., the structural properties of a glass at zero temperature [9], but also for making in contact the structural properties with the dynamical ones, i.e., the relaxation towards the inherent state. Since random pinning naturally introduce such a length scale $\xi^3 \propto pN$, we can then extract the behavior of ξ as a function of temperature just comparing $s(p, T^* = \infty) \equiv s(p)$ with $s(T^*, p = 0) \equiv s(T)$. Moreover, we showed that the same mapping can be done through other observables $\mathcal{O}(T, p)$ like the distribution of the displacement Δr performed by each particle for achieving the inherent structure. In particular, the behavior of ξ as a function of T obtained with considering $\mathcal{O}(T^*, p = 0) = \mathcal{O}(T^* = \infty, p)$ with $\mathcal{O} = \sigma_1$ and $\mathcal{O} = \sigma_2$ are consistent with the previous estimate of ξ .

In conclusion, $D(\omega)$ provides crucial information not only for understanding the anomalies of a glass with respect to a crystal, and thus when it looks like an anomalous solid. From $D(\omega)$ we can also extract important information about the correlation length of the heterogeneous regions in supercooled liquids, which, most likely, are the ultimate origin of the instability giving rise to the non-Goldstone modes [31–37]. As a future direction, it would be interesting to explore possible connections with recent experiments on the energy landscape in geologically hyperaged ambers [38].

Acknowledgments. GP acknowledges the financial support of the Simons Foundation (Grant No. 454949, Giorgio Parisi). This project has received funding from the European Research Council (ERC) under the European Unions Horizon 2020 research and innovation program (grant agreement No [694925]). This work was also supported by the Joint Laboratory on “Advanced and Innovative Materials”, ADINMAT, WIS-Sapienza (GP and MP).

[1] C. Kittel, *Introduction to solid state physics* (Wiley, 2005).

[2] R. C. Zeller and R. O. Pohl, Phys. Rev. B **4**, 2029 (1971), URL <https://link.aps.org/doi/10.1103/PhysRevB.4.2029>.

[3] V. Gurarie and J. T. Chalker, Phys. Rev. B **68**, 134207 (2003), URL <https://link.aps.org/doi/10.1103/PhysRevB.68.134207>.

[4] M. Baity-Jesi, V. Martín-Mayor, G. Parisi, and S. Perez-Gaviro, Phys. Rev. Lett. **115**, 267205 (2015), URL <https://link.aps.org/doi/10.1103/PhysRevLett.115.267205>.

[5] E. Lerner, G. Düring, and E. Bouchbinder, Phys. Rev. Lett. **117**, 035501 (2016), URL <https://link.aps.org/doi/10.1103/PhysRevLett.117.035501>.

[6] H. Mizuno, H. Shiba, and A. Ikeda, Proceedings of the National Academy of Sciences **114**, E9767 (2017), <http://www.pnas.org/content/114/46/E9767.full.pdf>, URL <http://www.pnas.org/content/114/46/E9767.abstract>.

[7] E. Lerner and E. Bouchbinder, Phys. Rev. E **96**, 020104 (2017), URL <https://link.aps.org/doi/10.1103/PhysRevE.96.020104>.

[8] L. Gartner and E. Lerner, SciPost Phys. **1**, 016 (2016), URL <https://scipost.org/10.21468/SciPostPhys.1.2.016>.

[9] L. Angelani, M. Paoluzzi, G. Parisi, and G. Ruocco, Proceedings of the National Academy of Sciences **115**, 8700 (2018), ISSN 0027-8424, <http://www.pnas.org/content/115/35/8700.full.pdf>, URL <http://www.pnas.org/content/115/35/8700>.

[10] B. Bernu, J. P. Hansen, Y. Hiwatari, and G. Pastore, Phys. Rev. A **36**, 4891 (1987), URL <https://link.aps.org/doi/10.1103/PhysRevA.36.4891>.

[11] T. S. Grigera and G. Parisi, Phys. Rev. E **63**, 045102 (2001), URL <https://link.aps.org/doi/10.1103/PhysRevE.63.045102>.

[12] J.-F. Bonnans, J. C. Gilbert, C. Lemaréchal, and C. A. Sagastizábal, *Numerical optimization: theoretical and practical aspects* (Springer Science & Business Media, 2006).

[13] R. Bell and P. Dean, Discussions of the Faraday society **50**, 55 (1970).

[14] U. Buchenau, N. Nücker, and A. Dianoux, Physical Review Letters **53**, 2316 (1984).

[15] K. Binder and W. Kob, *Glassy materials and disordered solids: An introduction to their statistical mechanics* (World Scientific, 2011).

[16] C. Cammarota and G. Biroli, Proceedings of the National Academy of Sciences **109**, 8850 (2012).

[17] S. Franz, EPL (Europhysics Letters) **73**, 492 (2006).

[18] G. Szamel and E. Flenner, EPL (Europhysics Letters) **101**, 66005 (2013), URL <http://stacks.iop.org/0295-5075/101/i=6/a=66005>.

[19] C. Cammarota and G. Biroli, The Journal of chemical physics **138**, 12A547 (2013).

[20] P. Scheidler, W. Kob, K. Binder, and G. Parisi, Philosophical Magazine B **82**, 283 (2002), <https://doi.org/10.1080/13642810208221307>, URL <https://doi.org/10.1080/13642810208221307>.

[21] G. Biroli, J.-P. Bouchaud, A. Cavagna, T. S. Grigera, and P. Verrocchio, Nature Physics **4**, 771 (2008).

[22] M. Ozawa, W. Kob, A. Ikeda, and K. Miyazaki, Proceedings of the National Academy of Sciences **112**, 6914 (2015).

[23] W. Kob, S. Roldán-Vargas, and L. Berthier, Nature Physics **8**, 164 (2012).

[24] C. Brito, G. Parisi, and F. Zamponi, Soft Matter **9**, 8540 (2013).

[25] K. H. Nagamanasa, S. Gokhale, A. Sood, and R. Ganapathy, Nature Physics **11**, 403 (2015).

[26] S. Karmakar and G. Parisi, Proceedings of the National Academy of Sciences **110**, 2752 (2013).

[27] S. Chakrabarty, S. Karmakar, and C. Dasgupta, Scientific reports **5**, 12577 (2015).

[28] W. Kob, C. Donati, S. J. Plimpton, P. H. Poole, and S. C. Glotzer, Phys. Rev. Lett. **79**, 2827 (1997), URL <https://link.aps.org/doi/10.1103/PhysRevLett.79.2827>.

[29] N. Laevi, F. W. Starr, T. B. Schrder, and S. C. Glotzer, The Journal of Chemical Physics **119**, 7372 (2003), <https://doi.org/10.1063/1.1605094>, URL <https://doi.org/10.1063/1.1605094>.

[30] L. Berthier and G. Biroli, Rev. Mod. Phys. **83**, 587 (2011), URL <https://link.aps.org/doi/10.1103/RevModPhys.83.587>.

[31] W. Schirmacher, EPL (Europhysics Letters) **73**, 892 (2006).

[32] W. Schirmacher, G. Ruocco, and T. Scopigno, Physical review letters **98**, 025501 (2007).

[33] W. Schirmacher, B. Schmid, C. Tomaras, G. Viliani, G. Baldi, G. Ruocco, and T. Scopigno, physica status solidi c **5**, 862 (2008).

[34] A. Marruzzo, S. Köhler, A. Fratalocchi, G. Ruocco, and W. Schirmacher, The European Physical Journal Special Topics **216**, 83 (2013).

[35] A. Marruzzo, W. Schirmacher, A. Fratalocchi, and G. Ruocco, Scientific reports **3** (2013).

[36] C. Tomaras and W. Schirmacher, Journal of Physics: Condensed Matter **25**, 495402 (2013).

[37] W. Schirmacher, T. Scopigno, and G. Ruocco, Journal of Non-Crystalline Solids **407**, 133 (2015).

[38] E. A. A. Pogna, A. I. Chumakov, C. Ferrante, M. A. Ramos, and T. Scopigno, The Journal of Physical Chemistry Letters **0**, 427 (0), <https://doi.org/10.1021/acs.jpclett.9b00003>, URL <https://doi.org/10.1021/acs.jpclett.9b00003>.